On the ultraviolet photodissociation of H_2Te

Aleksey B. Alekseyev[a] and Heinz-Peter Liebermann
Fachbereich C—Theoretische Chemie, Bergische Universität Wuppertal, Gaussstrasse 20, D-42097 Wuppertal, Germany

Curt Wittig
Department of Chemistry, University of Southern California, Los Angeles, California 90089-0482

(Received 7 June 2004; accepted 5 August 2004)

The photodissociation of H_2Te through excitation in the first absorption band is investigated by means of multireference spin-orbit configuration interaction (CI) calculations. Bending potentials for low-lying electronic states of H_2Te are obtained in C_{2v} symmetry for Te-H distances fixed at the ground state equilibrium value of $3.14a_0$, as well as for the minimum energy path constrained to $R_1=R_2$. Asymmetric cuts of potential energy surfaces for excited states (at $R_1=3.14a_0$ and $\theta=90.3°$) are obtained for the first time. It is shown that vibrational structure in the 380–400 nm region of the long wavelength absorption tail is due to transitions to $3A'$, which has a shallow minimum at large HTe-H separations. Transitions to this state are polarized in the molecular plane, and this state converges to the excited $\mathrm{TeH}(^2\Pi_{1/2})+\mathrm{H}(^2S)$ limit. These theoretical data are in accord with the selectivity toward $\mathrm{TeH}(^2\Pi_{1/2})$ relative to $\mathrm{TeH}(^2\Pi_{3/2})$ that has been found experimentally for 355 nm H_2Te photodissociation. The calculated $3A'\leftarrow\tilde{X}A'$ transition dipole moment increases rapidly with HTe-H distance; this explains the observation of $3A'$ vibrational structure for low vibrational levels, despite unfavorable Franck–Condon factors. According to the calculated vertical energies and transition moment data, the maximum in the first absorption band at ≈245 nm is caused by excitation to $4A''$, which has predominantly $2\,^1A''$ ($^1B_1$ in C_{2v} symmetry) character. © *2004 American Institute of Physics.* [DOI: 10.1063/1.1799572]

I. INTRODUCTION

Experimental data have been obtained recently for the near ultraviolet photophysics and photochemistry of the H_2Te molecule.[1] The ultraviolet (UV) absorption spectrum of room temperature H_2Te has been measured, and photodissociation experiments have been carried out with expansion-cooled samples by using high-*n* Rydberg time-of-flight spectroscopy. It has been shown that the UV absorption spectrum has a long wavelength tail that extends up to 400 nm. Vibrational structure has been discovered in the 380–400 nm region of the long wavelength tail, and it has been interpreted as belonging to a shallow well in the adiabatic state that dissociates to the $\mathrm{TeH}(^2\Pi_{1/2})+\mathrm{H}(^2S)$ limit, analogous to the $^3\Pi_{0+}$ state in HI, which correlates to $\mathrm{I}(^2P_{1/2})+\mathrm{H}(^2S)$. Marked selectivity toward the $\mathrm{TeH}(^2\Pi_{1/2})$ excited spin state was observed for 355 nm photodissociation.

Altogether, the above findings led the authors of Ref. 1 to conclude that H_2Te might be a good photolytic source of tunable, monoenergetic H atoms with modest translational energies, from several hundred to several thousand wavenumbers. An important question arising from this work is whether the interpretation of the observed absorption spectrum and photodissociation mechanism, which is based on analogy with isoelectronic HI,[2,3] is correct. It is also interesting to understand the extent to which the trends observed in the 355 nm photodissociation of H_2Te can be extended to longer wavelengths and how intersections of potential surfaces at large HTe-H separations influence yields of dissociation products.

Clearly, comparisons with lighter Group VI A hydrides are useful. The lightest member of this group H_2O has been studied thoroughly, both experimentally and theoretically (see, for example, reviews[4,5] and references cited therein). The H_2S molecule has also been the subject of numerous experimental and theoretical studies (see, for example, Refs. 5–9 and references cited therein), whereas data on the absorption and photodissociation of the two heavier systems of this group, H_2Se and H_2Te, is relatively scarce.[10–12] At this point it is worth noting that there are significant differences even in the photodissociation of H_2O and H_2S. The H_2O molecule can be considered as a prototype for direct photodissociation of triatomic systems, while H_2S represents a case of electronic predissociation, with the participation of two potential energy surfaces (PESs). It is also noteworthy that some effects observed in H_2Te photodissociation[1] have no counterparts with the light Group VI A hydrides.

It is well known that relativistic effects are significant in systems that contain heavy atoms and that they have important influences on spectroscopy and photochemistry. For example, spin-orbit interaction makes many spin-forbidden transitions allowed, and it also couples various PESs, which can result in complicated intramolecular dynamics. Another issue, though not directly related to the relativistic character of systems with heavy atoms, but which nevertheless is very important, is the high density of electronic states at low excitation energies. This leads to a rich variety of intramolecular and dissociation processes within a relatively narrow en-

[a]Author to whom correspondence should be addressed. Electronic mail: alexeev@uni-wuppertal.de

ergy range. Therefore, the analogy between H_2Te photodissociation and the corresponding process in isoelectronic HI enlisted in Ref. 1 appears to be well grounded. On the other hand, the multidimensional character of the former system may lead to important distinctions.

From the above, it is clear that theoretical data are needed to advance our understanding of H_2Te photodissociation. The only *ab initio* study of H_2Te in which correlation and spin-orbit effects were treated was carried out by Sumathi and Balasubramanian.[13] Bending PESs were calculated in this work for the ground and low-lying excited states by optimizing the Te-H bond lengths for each bending angle θ. Though topologies for minimal energy paths along angle coordinates were analyzed and a number of molecular properties and parameters were determined, a reaction path for HTe-H dissociation was not studied.

The main goal of the present work is to obtain better insight into HTe-H photodissociation. Toward this end, *ab initio* calculations for the ground and lowest excited states of H_2Te are carried out to obtain PESs as well as transition dipole moments at selected geometries. On this basis, the first absorption band of H_2Te is analyzed, including possible decay channels. We concentrate here on the $TeH(^2\Pi) + H(^2S)$ dissociation path, because this is central to the interpretation of the experimental results.[1] Information on bending PESs has also been obtained and is compared with earlier theoretical data.[13]

II. COMPUTATIONAL METHOD

Relativistic configuration interaction (CI) calculations have been carried out for the ground and low-lying excited states of H_2Te. The core electrons of the tellurium atom are described by using a semicore relativistic effective core potential (RECP) (Ref. 14) so that only the $4d$, $5s$, and $5p$ electrons need to be treated explicitly in the ensuing self-consistent-field (SCF) and CI calculations. The $(5s5p3d)$ Gaussian functions with smallest exponents have been taken from the all-electron basis set for Te constructed in Ref. 15 and they are employed in uncontracted form. This set has been augmented by $1d\,(0.3a_0^{-2})$ and $1f\,(2.5a_0^{-2})$ functions optimized in our earlier TeH study.[16] The atomic orbital (AO) basis set for the hydrogen atom is the $(8s2p)/[5s2p]$ set of Woon and Dunning[17] augmented by diffuse s (0.0195) and p (0.042) functions.

The first step in the theoretical treatment is to carry out an SCF calculation for the $\tilde{X}^1A_1$ ground state in C_{2v} symmetry or for $\tilde{X}^1A'$ in C_s point group in the general case of unequal Te-H distances. In all calculations, the H_2Te molecule is located in the x-z-plane, with z chosen as the symmetry axis in the C_{2v} group. The ground state corresponds to the $\ldots 1a_1^2 1b_2^2 2a_1^2 1b_1^2$ electronic configuration (the lowest molecular orbitals (MOs) contaning ten d electrons of Te are omitted in this notation). The next step is to carry out a series of multireference single- and double-excitation CI (MRD-CI) calculations for several lowest roots of each Λ-S symmetry. Numbers of roots treated and reference configurations employed in calculations of bending potentials in C_{2v} symmetry are given in Table I along with the corresponding orders of the secular equations solved and the sizes of the $T=0$ CI spaces considered. The CI calculations are carried out with a standard perturbative selection procedure[18] for a threshold of $T=0.5\mu E_h$. The MOs corresponding to the Te $4d$ electrons also are included in the CI excitation space so that the complete number of active electrons is 18. The Table-CI algorithm[19] is employed to compute Hamiltonian matrix elements between the many-electron basis functions and a Direct-CI technique[20] is used to obtain the energy eigenvalues and eigenvectors for the various Λ-S states. The multireference Davidson correction[21,22] is also applied for each root in order to obtain an estimate of the effect of higher excitations on the computed energies, while molecular properties such as electric dipole and transition moments are calculated with the variational CI wave functions.

TABLE I. Technical details of the MRD-CI calculations in C_{2v} symmetry at $T=0.5\mu E_h$. The numbers of selected SAFs are given for $R=3.14a_0$ and $\theta=90.3°$. SAFTOT designates the total number of generated SAFs, SAFSEL—the number of selected SAFs, N_{ref} and N_{root} refer to the number of reference configurations and roots treated, respectively.

C_{2v}	N_{root}	N_{ref}	SAFTOT	SAFSEL	$D_{\infty h}$	C_s
$^1A_1$	3	58	5 855 676	128 783	$^1\Sigma_g^+$	$^1A'$
					$^1\Pi_u$	$^1A'$
$^1A_2$	2	43	5 611 032	108 744	$^1\Pi_g$	$^1A''$
					$^1\Sigma_g^-$	$^1A''$
$^1B_1$	3	46	5 402 549	142 163	$^1\Pi_u$	$^1A''$
					$^1\Delta_g$	$^1A''$
$^1B_2$	3	46	5 382 632	181 984	$^1\Pi_g$	$^1A'$
$^3A_1$	3	71	17 360 231	223 167	$^3\Pi_u$	$^3A'$
$^3A_2$	2	43	10 250 554	151 395	$^3\Pi_g$	$^3A''$
$^3B_1$	3	46	9 764 504	201 639	$^3\Pi_u$	$^3A''$
					$^3\Delta_g$	$^3A''$
$^3B_2$	3	46	9 722 690	270 405	$^3\Pi_g$	$^3A'$

The calculations of the H_2Te bending PESs have been carried out in the C_{2v} point group at the Λ-S level of treatment, i.e., without including spin-orbit (SO) coupling. As can be shown, the influence of the latter is relatively small in the Franck–Condon region, but becomes important at small bending angles, where it is responsible for avoided crossings between various Λ-S states and thus for potential barriers in the insertion reaction paths. Such PESs are not relevant to the HTe-H dissociation path, however. The corresponding calculations are quite time consuming and they will be the subject of a future study. On the contrary, accounting for SO interaction is absolutely crucial for analysis of the HTe-H photodissociation process, and it is performed in the present calculations in the C_s double group.

The technique for including spin-orbit coupling in the present treatment involves forming a matrix representation of the full relativistic Hamiltonian in the basis of the Λ-S wave functions obtained first. It can be viewed as a CI method employing a heavily contracted many-electron basis. It works especially well in applications such as the present one, in which spin-orbit interaction is essential but of secondary importance compared to terms in the nonrelativistic Hamiltonian [Λ-S contracted SO-CI or simply LSC-SO-CI (Refs. 23 and 24)]. It should be noted that in this procedure the diagonal Hamiltonian matrix elements do not have spin-orbit

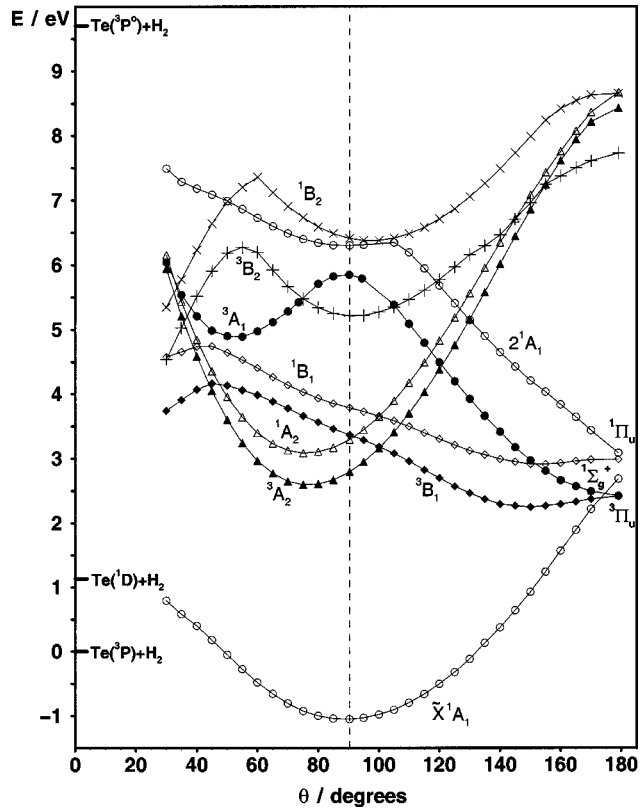

FIG. 1. Bending PESs for the low-lying states of H_2Te computed at $R=3.14a_0\simeq R_e(\tilde{X}^1A_1)$ without including spin-orbit coupling. The vertical dashed line indicates an equilibrium angle ($\theta=90.3°$) for the ground state.

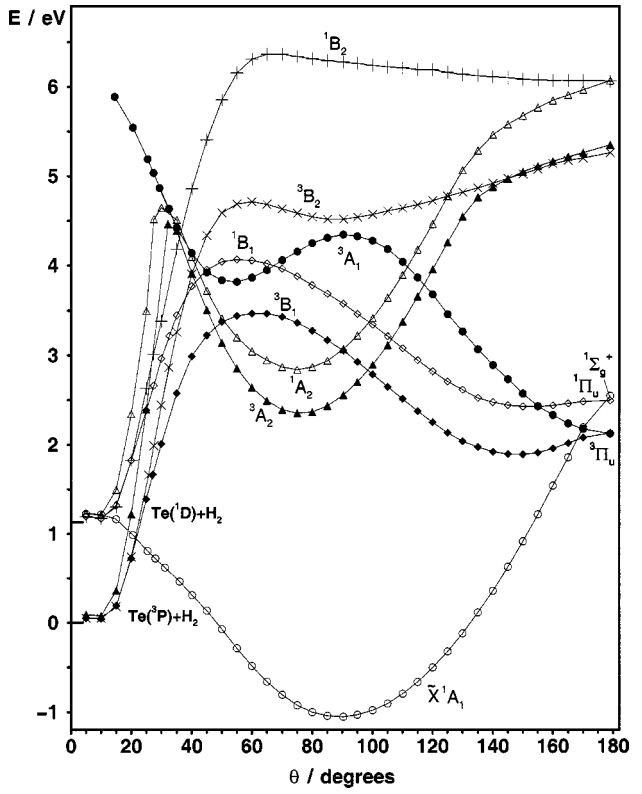

FIG. 2. Minimal energy path PESs for the low-lying states of H_2Te computed in C_{2v} symmetry without including spin-orbit coupling.

contributions and are simply the energy eigenvalues of the various Λ-S wave functions. For this purpose the estimated full CI results are used, that is, to which the Davidson correction has been applied.[21,22] The calculations in the C_s point group have been carried out for two to four lowest roots for each of the four $^{1,3}A'$ and $^{1,3}A''$ symmetries at $T=0.2\mu E_h$. The characteristic dimensions are $(20-60)\times10^6$ for total number of symmetry adapted functions (SAFs) and $(1-3)\times10^5$ for selected SAFs depending on irredicable representation and geometry. The off-diagonal spin-orbit matrix elements are computed with the variational eigenfunctions. The above procedure has also an advantage of providing a direct analysis of the final spin-perturbed electronic wave functions in terms of its Λ-S components. Transition moments between the final double group symmetry states are obtained by transformation of the corresponding Λ-S results mentioned above. A critical review of the LSC-SO-CI computational procedure as well as of the more demanding MR-SO-CI approach, in which Coulomb, exchange and spin-orbit interactions are treated at an equal footing, has been given earlier,[23] while its applications to computation of photodissociation processes have been presented in Refs. 2, 3, and 25.

III. RESULTS AND DISCUSSION

A. Bending potential energy curves

Bending potentials for some low-lying states that have been calculated without the inclusion of spin-orbit interaction are shown in Fig. 1. Both of the Te-H distances are fixed at the approximate $\tilde{X}^1A_1$ equilibrium value of $3.14a_0$. The calculated equilibrium parameters for the ground state are $R_e=3.137a_0$ and $\theta_e=90.30°$, in excellent agreement with the experimental values of $3.135a_0$ and 90.26°.[26] As the bending angle is decreased below 30°, the potential energies of all of the states under consideration increase rapidly due to repulsion between the H atoms. Such geometries are not of interest to us here, so they are not shown in Fig. 1. To describe H_2-Te dissociation, PESs are calculated at simultaneously increasing H-Te distances. These data are shown in Fig. 2, which depicts minimal energy paths for each state in C_{2v} symmetry, i.e., with both Te-H distances equal and optimized for each value of θ. Small angles correspond in this case to large Te-H separations and consequently they correspond to the Te atom approaching the H_2 molecule. The calculated geometries and energies for selected regions of the PESs are presented in Table II where they are compared with results of earlier calculations.[13]

The $\tilde{X}^1A_1(\ldots1a_1^21b_2^22a_1^21b_1^2)$ ground state correlates with insertion of Te(^1D) into H_2. The binding energy with respect to Te(^1D)+H_2 is computed to be 2.29 eV=18 450 cm^{-1}. This is obtained without SO coupling; it will increase slightly with the inclusion of SO interaction, mainly due to the Te($^1D_2$-$^3P_2$) repulsion at the dissociation limit and partly due to a small lowering of the $\tilde{X}^1A_1$ minimum. As seen in Fig. 2, the linear geometry is quite unfavourable for the $\tilde{X}^1A_1$ ground state (which is of $^1\Sigma_g^+$ symmetry in the $D_{\infty h}$ point group), with an energy that is 3.60 eV=29 000 cm^{-1} higher than that of the bent minimum.

The lowest excited states of H_2Te in the Franck–Condon

TABLE II. MRD-CI geometries and energies for selected features in the bending potentials of H_2Te. All energies are given with respect to the global minimum of the $\tilde{X}^1A_1$ ground state. Notation min and max used in the second column corresponds to the local extrema in the Λ-S bending PESs.

		θ (deg.)		R_e (Å)		E (eV)	
State		This work	a	This work	a	This work	a
$\tilde{X}^1A_1$	min	90.3[b]	91.2[c]	1.660	1.668	0	0
		180.0		1.905	1.977	3.60	3.45
Expt.[d]		90.26		1.659			
$^3A_2$	min	76.1	76.4	1.811	1.820	3.42	3.27
	max	32.5				5.52	
		180.0		2.514		6.40	
$^1A_2$	min	74.1	72.5	1.811	1.912	3.90	3.64
	max	30.0				5.70	
		180.0		2.514		7.12	
$^3B_1$	max	62.5	60.0	1.942	2.111	4.52	4.63
	min	148.9		1.835		2.94	
		180.0		1.799	1.879	3.18	3.20
$^1B_1$	max	55.6	53.5	1.947	2.224	5.12	5.19
	min	153.9		1.876		3.47	
		180.0		1.852	1.977	3.55	3.45
$^3A_1$	min	54.1		2.047		4.87	
	max	90.7		2.196		5.40	
		180.0		1.799		3.18	

[a]Reference 13.

[b]Equilibrium geometry for the $\tilde{X}^1A_1$ state has been obtained in this study in the LSC-SO-CI calculations including SO coupling, for all other states—at the Λ-S level of treatment.

[c]The data from Ref. 13 presented here for $\tilde{X}^1A_1$, $^3A_2$, and $^1A_2$ were obtained in the second-order CI (SOCI) calculations, for all other states—in the CASSCF calculations.

[d]Reference 26.

region are $^3A_2$ and $^1A_2$, with excitation energies of 27 620 and 31 470 cm^{-1}, respectively. These states correspond to electron excitation from the lone pair $1b_1$ orbital to the antibonding $2b_2$ orbital. Their local potential minima lie at smaller angles than that of the ground state, i.e., 76.1° and 74.1°, respectively, vs 90.3°. Though the $^3A_2$ state converges to the lowest dissociation limit, $Te(^3P)+H_2$, to reach this limit a high barrier at $\theta=35°$ must be overcome (Fig. 2). The $^1A_2$ state is characterized by a similar minimal energy cut along the angle coordinate, but it converges to the $Te(^1D)+H_2$ limit, with the barrier located at ≈30°. As with the ground state, linear geometries of both of these A_2 states are characterized by much higher energies. It will be shown in the following section that the $^1A_2$ and $^3A_2$ states are repulsive with respect to another process—dissociation to $TeH(^2\Pi)+H(^2S)$.

The excited states $^3B_1$ and $^1B_1(1b_1\rightarrow 3a_1)$ are characterized by very different PESs than the states discussed above. They also have barriers on the $Te(^3P,^1D)+H_2$ reaction paths, but their minima are shifted towards linear geometries, lying at 148.9° and 153.9° for $^3B_1$ and $^1B_1$, respectively. The corresponding energies (Fig. 2) are lower than those of the $^1A_2$ and $^3A_2$ states, and we shall see that this influences HTe-H dissociation. As pointed out in Ref. 13, the $^3A_1(1b_1\rightarrow 2b_1)$ state arises from reaction of the highly excited $Te(5s^15p^5\,^3P^\circ)$ atom with H_2, which is an example of the exothermic process analogous to the H_2Te ground state case. This state has a local minimum at $\theta=54.1°$, whereas its global minimum is linear.

Good overall agreement of the bending potentials calculated in this work with the earlier theoretical data of Sumathi and Balasubramanian[13] is noted, with all of the important topological features being confirmed in the present calculations. The characteristic bending angles and excitation energies obtained in both studies agree quite well (see Table II), while the Te-H bond lengths determined in this work for extrema of various states are somewhat smaller than those of Ref. 13. New theoretical data are presented here for the $^3B_2$ and $^1B_2$ states.

B. Asymmetric stretch potential energy curves

Asymmetric stretch potential energy curves calculated at the Λ-S level, i.e., without spin-orbit interaction, are shown in Fig. 3. These are cuts of PESs along one Te-H distance coordinate, with the other distance and the bending angle held fixed at the ground state equilibrium values of $3.14a_0$ and 90.3°. It should be noted that fixing one distance at the equilibrium value for the H_2Te ground state is appropriate for HTe-H dissociation, because R_e for the $TeH(^2\Pi_{3/2})$ ground state[16] is only 0.003 Å smaller than R_e for H_2Te. As seen in the preceding section, changes in the bending angle, though important for the dissociation dynamics, play a less significant role in photoexcitation.

In the Franck–Condon region, the lowest excited state is $^3A''$ ($^3A_2$ in C_{2v} symmetry) followed by $^1A''(^1A_2)$, which lies ≈4000 cm^{-1} higher. The $^3A''$ state has a shallow minimum of ~140 cm^{-1} at $R\sim 5.0a_0$, while $^1A''$ is purely repulsive along this cut. One more state converges to the same $TeH(^2\Pi)+H(^2S)$ limit, $1^3A'$, which is purely repulsive as

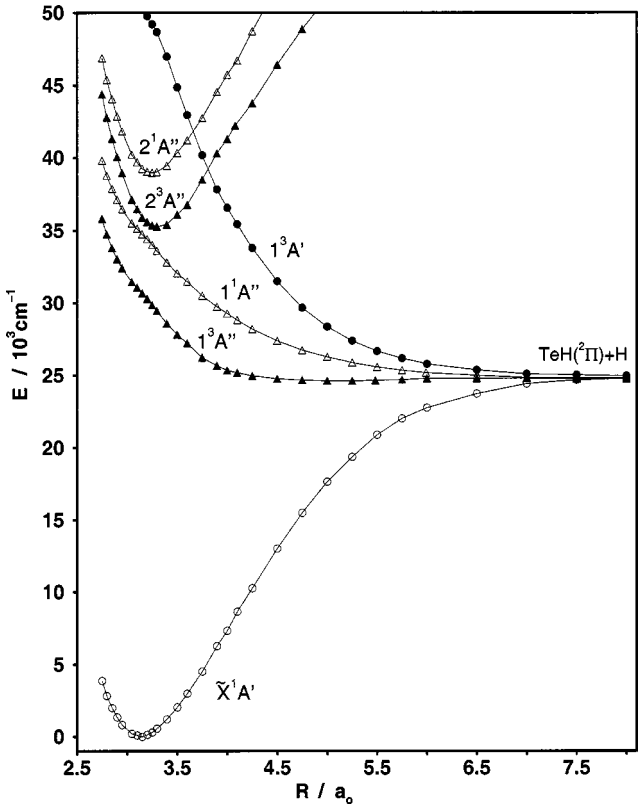

FIG. 3. Computed asymmetric stretch PESs for the low-lying states of H_2Te obtained for $R_1=3.14a_0$ and $\theta=90.3°$ without including spin-orbit coupling.

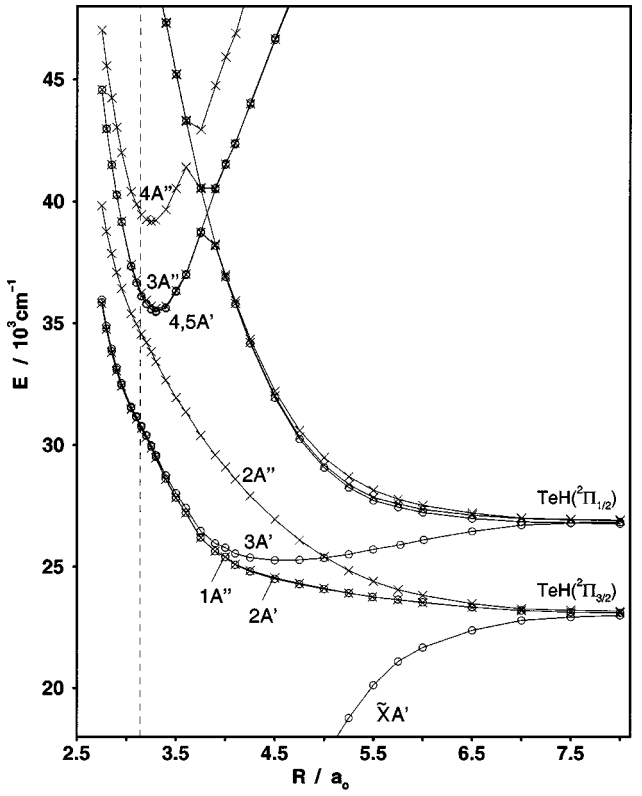

FIG. 4. Computed asymmetric stretch PESs for the low-lying states of H_2Te obtained at $R_1=3.14a_0$ and $\theta=90.3°$ with spin-orbit coupling. The vertical dashed line indicates the equilibrium distance of the ground state.

well and lies significantly higher in the Franck–Condon region, at least at the geometries of interest here.

The $2^3A''$ state ($^3B_1$ in the C_{2v} point group) lies only 1200 cm^{-1} above $1^1A''$ at the ground state equilibrium geometry and is followed by $2^1A''(^1B_1)$. As seen in Fig. 3, each of these states is bound at the bent geometry with respect to HTe-H dissociation.

Asymmetric stretch potentials calculated with the inclusion of SO coupling are shown in Fig. 4. The influence of SO coupling on the $\tilde{X}^1A'$ ground state is small in the Franck–Condon region (lowering $\tilde{X}^1A'$ by $\approx$200 cm^{-1}), whereas at large TeH-H separations it is $\sim$1900 cm^{-1}, i.e., approximately half of the TeH($^2\Pi$) splitting. This leads to a decrease of the computed $\tilde{X}^1A'$ dissociation energy. The D_e value for the ground state is calculated by averaging energies of four states that converge to the Te($^2\Pi_{3/2}$) limit at $R=8a_0$ and it is found to be 23 070 cm^{-1}, which is 0.12 eV higher than 2.74 eV computed earlier.[13] If the experimental vibrational frequencies for H_2Te ($\omega_1=2065\,cm^{-1}$—symmetric stretch, $\omega_2=861\,cm^{-1}$—bending, and $\omega_3=2072\,cm^{-1}$—antisymmetric stretch[27,28]) and HTe [ω=2137 cm^{-1} (Ref. 29)] are used, one gets $D_0=21\,640\,cm^{-1}$. This value is about 0.14 eV too small in comparison with the experimental result $D_0=22\,740\,cm^{-1}$ (Ref. 1), which is typical for calculations with the type of basis set employed. For the TeH $^2\Pi_{1/2}$-$^2\Pi_{3/2}$ splitting, determined in a similar way, a value of 3800 cm^{-1} has been obtained, in agreement with the experimental value of 3816 cm^{-1}.[16]

The first excited Λ-S state $^3A''$ is split into $A'+A''+A'$ components, the lowest two of which $2A'$ and $1A''$ converge to the TeH($^2\Pi_{3/2}$) limit and are repulsive. The SO splitting between them is small: $<$70 cm^{-1} for all HTe-H separations.

An interesting low energy state is $3A'$. A cut of its PES at fixed values of $R_1=3.14a_0$ and $\theta=90.3°$ reveals a shallow well (1620 cm^{-1}) at $R_2\sim4.6a_0$. In consideration of the vibrational frequency of 330 cm^{-1} estimated in the experimental study,[1] this well supports a small number of vibrational levels. We believe that these correspond to the peaks observed in the long wavelength tail of the absorption spectrum, i.e., at 395, 389.5, 384.5, 380, and 377 nm [Ref. 1, Fig. 1(b)]. In addition, the calculated energy of the $3A'$ minimum is 25 220 cm^{-1} above the ground state. When including the difference between the zero-point energies of $3A'$ and the ground state and taking into account some underestimation of the ground state binding energy, this value is consistent with the observed vibrational levels.

From the above computed data, it can be concluded that excitation to $3A'$ is responsible for vibrational structure in the 380–400 nm range of the absorption spectrum. In addition, preliminary calculations have shown that the absolute minimum of $3A'$ lies at $R_2\simeq4.40a_0$ and $\theta\simeq78°$, and is $\approx$160 cm^{-1} deeper than the above value of 1620 cm^{-1}. It is also worth noting the qualitative similarity in the photodissociation of H_2Te and isoelectronic HI,[1–3] with $3A'$ being the analog of the $^3\Pi_{0+}$ state in HI.

The fact that H_2Te is polyatomic has important conse-

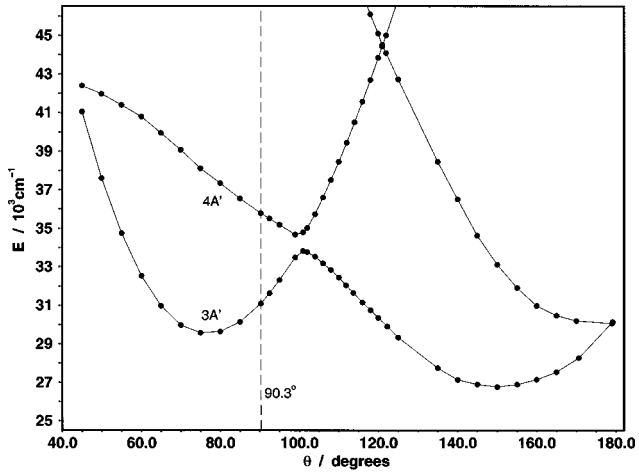

FIG. 5. Bending PESs for the $3A'$ and $4A'$ states of H_2Te computed including spin-orbit coupling at $R_1=R_2=3.14a_0$ in C_s double group. The vertical dashed line indicates the equilibrium angle ($\theta=90.3°$) of the ground state.

quences for dissociation dynamics. As seen in Fig. 2, $^3B_1$ ($2^3A''$ in the C_s point group) has a minimum at large bending angles that lies lower than the $^3A_2(1^3A'')$ minimum. Both of these Λ-S states have A' components ($3A'$ and $4A'$, both of A_1 symmetry in the C_{2v} double group) that nearly intersect conically on their way to dissociation. This is illustrated in Fig. 5, which depicts calculated cuts (that include spin-orbit interaction) for $3A'$ and $4A'$ at $R_1=R_2=3.14a_0$.

Figure 5 shows that the avoided crossing yields an adiabatic $3A'$ PES that has two minimum energy paths to products. In terms of two-dimensional (R_2 and θ) PESs, there are two valleys with a sharp ridge separating them. Vertical excitation from the ground state ($\theta\sim90°$) accesses the positive slope of the left valley and dissociation occurs concomitantly with bending and asymmetric stretch motions that depend on the excitation energy. Because the height of the ridge between the valleys decreases as R_2 increases, dissociation may also access the large-θ valley of the A' PES. Accurate analyses of the dissociation dynamics will require multidimensional *ab initio* PESs, and this work is in progress.

The avoided crossing shown in Fig. 5 yields a minimum on the adiabatic $4A'$ PES at $\sim100°$. An additional crossing, this time a real conical intersection between $A_1(^3A_2)$ and $B_2(^3A_1)$ in C_{2v} symmetry, results in the adiabatic $4A'$ state having a minimum at linear geometries. Because the adiabatic $3A'$ and $4A'$ each converges to the same limit at large R_2 transitions between them do not change the respective quantum yields of the TeH spin-orbit states. Such transitions may, however, influence TeH vibrational and rotational excitations.

With regards to dissociation products, it is seen that $3A'$ and $2A''$ cross at fairly large R_2 and with quite different gradients (Fig. 4). Coupling occurs via Coriolis interaction, and numerical data can only be obtained in calculations of the multidimensional decay dynamics. Given that the photodissociation experiments have been carried out with rotationally cold molecules, interaction between these surfaces is not expected to be significant.

TABLE III. Vertical excitation energies, minimal energies for the PES cuts at $R_1=3.137a_0$, $\theta_e=90.3°$, transition dipole moments from the ground state and composition of the low-lying Ω states of H_2Te. Vertical excitations energies are calculated at the equilibrium geometry of the ground state: $R_1=R_2=3.14a_0$ and $\theta_e=90.3°$.

State	E (cm^{-1})	R_{min} (a_0)	μ (ea_0)	Composition of states[a]
$\tilde{X}A'$	0			99.5% $1\,^1A'$
$1A''$	30 842		0.0053	99.0% $1^3A''$, 0.6% $1^3A'$
$2A'$	30 909		0.0154	98.1% $1^3A''$, 0.8% $2^3A''$
$3A'$	30 942		0.0144	98.7% $1^3A''$, 1.1% $2^3A''$
	25 220	4.60	0.1364	96.8% $1^3A''$, 3.0% $1^1A'$
$2A''$	34 713		0.0	83.6% $1^1A''$, 15.4% $2^3A''$
				0.9% $1^3A'$
$4A'$	36 275		0.0402	0.8% $1^3A''$, 98.8% $2^3A''$
	35 621	3.30	0.0663	
$5A'$	36 287		0.0867	1.1% $1^3A''$, 98.8% $2^3A''$
	35 649	3.30	0.0606	
$3A''$	36 408		0.0	15.3% $1^1A''$, 84.6% $2^3A''$
	35 728	3.30	0.0509	
$4A''$	39 572		0.6811	99.7% $2^1A''$
	39 264	3.25	0.6299	

[a]Only contributions larger than 0.5% are presented.

C. Transition moments and composition of states

Referring to Fig. 4, nine electronic states have vertical excitation energies below 40 000 cm^{-1}, five A' and four A''. In order to understand which states are photoexcited efficiently, it is helpful to know the corresponding transition dipole moments μ that connect these states with the ground state. The computed vertical energies and μ values are given in Table III for the ground state equilibrium geometry, as well as for $R_1=3.14a_0$, $\theta=90.3°$, and R_2 distances, at which the excited states under consideration have their minima along the asymmetric stretch coordinate.

These data indicate that transitions to the two lowest excited A' states ($2A'$ and $3A'$) and the lowest A'' state ($1A''$) are weak ($\mu<0.02ea_0$) in the middle of the Franck–Condon region. This is not surprising, because these states originate from $1^3A''$ (see the compositions of states in the last column of Table III), and the $1^3A''$-$^1A'$ transition is spin forbidden. There is, however, an important distinction in the variation of the corresponding transition moments with HTe-H distance. Whereas transitions to $2A'$ and $1A''$ remain weak, the $3A'$-$1A'$ transition moment increases quickly with distance. It can be seen from Table III that this is due mainly to increased mixing of $1^3A''$ and $1^1A'$, although contributions from higher-lying states, in particular from the $3^1A'$ admixture to the $3A'$ state, are important as well. This explains why even low vibrational levels of $3A'$ were observed in absorption [Fig. 1(b) in Ref. 1], despite unfavorable Franck–Condon factors.

The weakness of the $2A''\leftarrow\tilde{X}A'$ transition at the $R_1=R_2$ geometry is also easy to understand. It corresponds to the $1^1A_2\leftarrow\tilde{X}^1A_1$ transition in the C_{2v} point group and is thus symmetry forbidden. The same is also true for the $3A''\leftarrow\tilde{X}A'$ transition, but in this case one has to think in terms of the C_{2v} double group. The $3A''$ state transforms according to the A_2 irreducible representation of this group and therefore its excitation from the $\tilde{X}A_1$ ground state is once again sym-

metry forbidden. It is also clear that when the H_2Te symmetry is reduced to C_s, both these transitions become allowed and preliminary calculations have shown that an absolute value of the $2A''\leftarrow\tilde{X}A'$ transition moment increases fairly fast to the left and to the right of the $R_1=R_2$ cut. This means that it can give a notable contribution to the continuous absorption spectrum at energies higher and lower than that of the vertical excitation ($\sim$34 700 cm^{-1}).

From the μ data presented in Table III, it is seen that strong absorption with a maximum at $\sim$245 nm and diffuse vibrational structure [Fig. 1(a) in Ref. 1] is caused by excitation to $4A''$. This transition is polarized perpendicular to the molecular plane, and this result is supported by the experimental measurements.[1] The $4A''\leftarrow\tilde{X}A'$ transition can explain the observed vibrational features of the absorption spectrum in the 232–254 nm (43 200–39 400 cm^{-1}) interval. The origin of the peaks at longer wavelengths, 260–290 nm (38 300–34 500 cm^{-1}), is less clear, but according to Table III the most probable candidates for explaining these observations are $4A'$ and $5A'$, though transitions to $2A''$ and $3A''$ may also be involved.

One should keep in mind that the present analysis is based mainly on PES cuts at the ground state equilibrium values of R_1 and θ, whereas for accurate calculation of the absorption spectra multidimensional data for potential energies and transition moments are needed. Such data must be obtained in *ab initio* treatments that include spin-orbit coupling, which make such calculations at a large grid time consuming.

IV. CONCLUSION

Multireference spin-orbit CI calculations are reported for low-lying electronic states of H_2Te. Bending potentials are obtained in C_{2v} symmetry for Te-H distances fixed at the ground state equilibrium value of $3.14a_0$, as well as for the minimum energy path constrained to $R_1=R_2$. Asymmetric PES cuts (at $R_1=3.14a_0$ and $\theta=90.3°$) for excited states also are obtained.

Emphasis is placed on the absorption spectrum and photodissociation pathways. It is shown that vibrational structure in the 380–400 nm region of the long wavelength absorption tail is due to transitions to $3A'$, which has a shallow minimum at large HTe-H separations. Transitions to this state are polarized in the molecular plane, and this state converges to the excited $TeH(^2\Pi_{1/2})+H(^2S)$ limit. These theoretical data are in accord with the selectivity toward $TeH(^2\Pi_{1/2})$ relative to $TeH(^2\Pi_{3/2})$ that has been found experimentally for 355 nm H_2Te photodissociation. As suggested in Ref. 1, the situation is analogous to HI photodissociation, in which $^3\Pi_{0+}$ leads to $I(^2P_{1/2})$.[2,3]

The calculated $3A'\leftarrow\tilde{X}A'$ transition dipole moment increases rapidly with HTe-H distance, which is similar to $^3\Pi_{0+}\leftarrow\tilde{X}^1\Sigma^+$ excitation in HI.[2] This explains the observation of $3A'$ vibrational structure for low vibrational levels, despite unfavorable Franck–Condon factors. According to the calculated vertical energies and transition moment data, the maximum in the first absorption band at $\approx$245 nm is caused by excitation to $4A''$, which has predominantly $2^1A''$ Rydberg character.

Further insight into the details of the absorption spectrum and dynamics of HTe-H dissociation requires *ab initio* calculations of global potential energy surfaces in which all three degrees of freedom are treated. This work is in progress.

ACKNOWLEDGMENTS

The authors are grateful to Professor Per Jensen for useful discussions. The financial support of the Fonds der Chemischen Industrie is also gratefully acknowledged. One of the authors (C.W.) was supported in this work by the U.S. Department of Energy, Division of Basic Energy Sciences.

[1] J. Underwood, D. Chastaing, S. Lee, P. Boothe, T. C. Flood, and C. Wittig, Chem. Phys. Lett. **362**, 483 (2002).
[2] A. B. Alekseyev, H.-P. Liebermann, D. B. Kokh, and R. J. Buenker, J. Chem. Phys. **113**, 6174 (2000).
[3] N. Balakrishnan, A. B. Alekseyev, and R. J. Buenker, Chem. Phys. Lett. **341**, 594 (2001).
[4] V. Engel, V. Staemmler, R. L. Vander Wal *et al.*, J. Phys. Chem. **96**, 3201 (1992).
[5] R. Schinke, *Photodissociation Dynamics* (Cambridge University Press, Cambridge, 1993).
[6] L. C. Lee, X. Wang, and M. Suto, J. Chem. Phys. **86**, 4353 (1987).
[7] C. Y. R. Wu and F. Chen, J. Quant. Spectrosc. Radiat. Transf. **60**, 17 (1998).
[8] B. Heumann and R. Schinke, J. Chem. Phys. **101**, 7488 (1994).
[9] D. Simah, B. Hartke, and H.-J. Werner, J. Chem. Phys. **111**, 4523 (1999).
[10] D. C. Dobson, F. S. James, I. Safarik, H. E. Gunning, and O. P. Strausz, J. Phys. Chem. **79**, 771 (1975).
[11] C. F. Goodeve and N. O. Stein, Trans. Faraday Soc. **27**, 393 (1931).
[12] D. J. Little, R. J. Donovan, and R. J. Butcher, J. Photochem. **2**, 451 (1973).
[13] K. Sumathi and K. Balasubramanian, J. Chem. Phys. **92**, 6604 (1990).
[14] L. A. LaJohn, P. A. Christiansen, R. B. Ross, T. Atashroo, and W. C. Ermler, J. Chem. Phys. **87**, 2812 (1987).
[15] A. Strömberg, O. Gropen, and U. Wahlgren, J. Comput. Chem. **4**, 181 (1983).
[16] K. D. Setzer, E. H. Fink, A. B. Alekseyev, H.-P. Liebermann, and R. J. Buenker, J. Mol. Spectrosc. **206**, 181 (2001).
[17] D. E. Woon and T. H. Dunning, Jr., J. Chem. Phys. **99**, 1914 (1993).
[18] R. J. Buenker and S. D. Peyerimhoff, Theor. Chim. Acta **35**, 33 (1974); **39**, 217 (1975); R. J. Buenker, S. D. Peyerimhoff, and W. Butscher, Mol. Phys. **35**, 771 (1978).
[19] R. J. Buenker and R. A. Philips, J. Mol. Struct.: THEOCHEM **123**, 291 (1985).
[20] S. Krebs and R. J. Buenker, J. Chem. Phys. **103**, 5613 (1995).
[21] E. R. Davidson, in *The World of Quantum Chemistry*, edited by R. Daudel and B. Pullman (Reidel, Dordrecht, 1974), p. 17.
[22] G. Hirsch, P. J. Bruna, S. D. Peyerimhoff, and R. J. Buenker, Chem. Phys. Lett. **52**, 442 (1977); D. B. Knowles, J. R. Alvarez-Collado, G. Hirsch, and R. J. Buenker, J. Chem. Phys. **92**, 585 (1990).
[23] A. B. Alekseyev, H.-P. Liebermann, and R. J. Buenker, in *Recent Advances in Relativistic Effects in Chemistry*, edited by K. Hirao and Y. Ishikawa (World Scientific, Singapore, 2004), p. 65.
[24] R. J. Buenker, A. B. Alekseyev, H.-P. Liebermann, R. Lingott, and G. Hirsch, J. Chem. Phys. **108**, 3400 (1998).
[25] A. B. Alekseyev, H.-P. Liebermann, R. J. Buenker, N. Balakrishnan, H. R. Sadeghpour, S. T. Cornett, and M. J. Cavagnero, J. Chem. Phys. **113**, 1514 (2000).
[26] C. A. Mayhew and J. P. Connerade, J. Phys. B **19**, 3493 (1986).
[27] J.-M. Flaud, M. Betrencourt, Ph. Arcas, H. Bürger, O. Polanz, and W. J. Lafferty, J. Mol. Spectrosc. **182**, 396 (1997).
[28] J.-M. Flaud, Ph. Arcas, H. Bürger, O. Polanz, and L. Halonen, J. Mol. Spectrosc. **183**, 310 (1997).
[29] E. H. Fink, K. D. Setzer, D. A. Ramsay, and M. Vervloet, J. Mol. Spectrosc. **138**, 19 (1989).